



# D-mannitol sensor based on molecularly imprinted polymer on electrode modified with reduced graphene oxide decorated with gold nanoparticles

Maísa Azevedo Beluomini\*, José L. da Silva, Graziela Cristina Sedenho, Nelson Ramos Stradiotto

Analytical Chemistry Department, Chemistry Institute, Universidade Estadual Paulista (UNESP), Rua Prof. Francisco Degni, 55, 14800-060 Araraquara, SP, Brazil

## ARTICLE INFO

### Keywords:

D-mannitol  
Reduced graphene oxide  
Au nanoparticles  
Molecularly imprinted electrochemical sensor  
Electrochemical determination

## ABSTRACT

An electrochemical sensor for D-mannitol based on molecularly imprinted polymer on electrode modified with reduced graphene oxide decorated with gold nanoparticles was developed in this present work. The sensor was constructed for the first time via the electropolymerization of o-phenylenediamine (o-PD) over a surface containing reduced graphene oxide (RGO) and gold nanoparticles (AuNP) in the presence of D-mannitol molecules. The surface modification with AuNP/RGO-GCE facilitated the charge transfer processes of  $[\text{Fe}(\text{CN})_6]^{3-/4-}$ , which was used as an electrochemical probe. It also contributed meaningfully towards the increase in the surface/volume ratio, creating more locations for imprinting, and providing greater sensitivity to the sensor. The MIP/AuNP/RGO-GCE sensor was characterized by cyclic voltammetry (CV), electrochemical impedance spectroscopy (EIS), scanning electron microscope (SEM), atomic force microscope (AFM) and X-ray Photoelectron Spectroscopy (XPS). Important parameters that exert control over the performance of the molecularly imprinted sensor (such as number of cycles, pH, monomer and template concentration and extraction and rebinding conditions) were investigated and optimized. The imprinting factor was 4.9, showing greater response to the D-mannitol molecule compared to the interfering molecules. The limit of detection, limit of quantification and amperometric sensitivity were  $7.7 \times 10^{-13} \text{ mol L}^{-1}$ ,  $2.6 \times 10^{-12} \text{ mol L}^{-1}$  and  $3.9 \times 10^{10} \mu\text{A L mol}^{-1}$  ( $n=3$ ) respectively. The MIP/AuNP/RGO-GCE sensor was successfully applied towards the selective determination of D-mannitol in sugarcane vinasse, thus making it, in essence, a valuable tool for the accurate and reliable determination of this molecule.

## 1. Introduction

The attractiveness of low molecular weight carbohydrates, primarily as starting materials in organic synthesis, lies in their possession of suitable characteristics including high availability, purity, and low cost. Among these carbohydrates, one that deserves mentioning is D-mannitol, a polyhydroxylated compound which can be obtained from the reduction of carbohydrates [1]. This molecule is widely used for various commercial and scientific purposes including the organic synthesis of Tamiflu [2], the manufacture of dietetic products (because of its slightly sweet taste) in the food industry, as an excipient in tablets, medicament for the reduction of intracranial pressure in intracranial surgery [3] and anesthetic [1] in the pharmaceutical industry. Notwithstanding its clinical importance, high amounts of D-mannitol (1.4 g/kg body weight) may cause blood pressure change, mortality or neurological outcome [4]. Oddly enough, despite the indisputable relevance of this compound, to date relatively few methods have been developed and validated for its determination.

Thus, the development of new, sensitive and selective methods for its determination becomes essentially indispensable.

Several analytical methods have been reported for the determination of D-mannitol, including gas chromatography (GC) [5,6], high performance liquid chromatography with electrochemical detection (HPLC-PAD) [7–11] and capillary electrophoresis (CE) [12–14]. Although these techniques are found to be successful for the detection of D-mannitol, they, nonetheless, have many shortcomings. Some of these disadvantages include the high cost of the equipment, the complexity nature of the pre-treatment steps and the fact that the techniques require the use of well-trained professionals to operate them. Such reasons render the search for a good, efficient and relatively less costly method for the detection of D-mannitol essentially imperative.

Electrochemical sensors possess low cost, high sensitivity and short time analysis compared to the other common analytical techniques. Nonetheless, only few works have been published dealing with the electrochemical detection of D-mannitol [12,18–21], and no reports

\* Corresponding author.

E-mail address: [mabeluomini@gmail.com](mailto:mabeluomini@gmail.com) (M.A. Beluomini).

have been found in the literature concerning the use of specific sensors for the determination of D-mannitol in real samples. In this context, one of the electrochemical sensors that has drawn wider attention in recent years is based on molecularly imprinted polymers (MIP).

The search for new tailor-made sensors with high selectivity, sensitivity, great reliability, stability (mechanical, thermal and chemical), makes the molecular imprinting technique a promising mechanism suitable for achieving those goals [15,16]. The molecular imprinting process involves polymerization of functional monomers in the presence of the template molecule (usually the molecule of interest in the detection, or a molecule of similar size, and chemical functionality) [16] and subsequent template extraction from the polymer network. This process generates cavities that are capable of recognizing the target molecules selectively in any matrix of interest [17].

MIPs are commonly prepared by free radical polymerization, photopolymerization, and electropolymerization [18]. The merit of electropolymerization in comparison to other techniques lies in the possibility to control the thickness of the electrodeposited film and its morphology through electropolymerization conditions (e.g. applied voltage, cyclic scan). Hence, we chose the electropolymerization of o-phenylenediamine (o-PD) for the development of the sensor owing to the fact that this monomer has been widely used in electrochemical sensors based on MIP towards the growth of compact and thin films, required to provide a shorter response time for the sensor, with high thermostability and homogeneity [19].

The sensitivity of the molecularly imprinted sensor is related to the amount of effective imprint sites formed on the sensor surface. However, the MIPs are found to face many obstacles, especially when formed on planar electrodes, among such inhibitions include the lack of accessibility to imprinting sites, low removal of the template molecule formed, inhomogeneous formation of binding sites, agglomeration of cavities, irregular polymerization and slow transfer of electrons (low kinetic). Furthermore, the polymer interaction with the planar electrodes surface is often found to be poor, causing low electrochemical signal [20,21]. The formation of nanostructured surfaces appears to be a promising way if we are to circumvent these shortcomings.

Compared with planar surfaces, nanostructured surfaces can be constructed with high surface volume/ratio, increasing the number and proportion of imprinted locations that are accessible for binding, thus raising the capacity of the MIP in up to 15 times [22]. In this sense, some researchers have focused on the preparation of nanostructured MIPs using arrays that can further increase the amount of printing locations [15,23,24].

In recent times, graphene-based materials have attracted considerable interest on grounds of their novel characteristics, such as large specific surface area, high thermal and mechanical properties. Additionally, metallic nanoparticles are found to present excellent electrocatalytic performance and notable electrical conductivity, providing better electrochemical response (higher current response) to the sensor, making them a considerably ideal material for the preparation of chemical and biological sensors [23,25,26].

In this study, gold nanoparticles (AuNP) anchored on reduced graphene oxide (RGO) combined with the high selectivity of MIP for the determination of D-mannitol have been constructed for the first time. D-mannitol molecules were used as template molecule in the imprinting for their determination in sugarcane vinasse sample.

Vinasse has become an object of intense studies as a result of its effects on soil and groundwater, including water contamination, soil salinization and leaching of metals and sulphates [27]. Because of the large amount of vinasse produced by the sugarcane industry (14–15 l per liter of ethanol) [28], there has been a huge interest in developing a concept of biorefineries for the production of fuels and chemicals that provide economic, environmental and strategic advantages, as is the case of the D-mannitol molecule. Thus, it is deemed an interesting matrix for the implementation of the proposed method.

All the steps concerning the sensor fabrication were performed via

electrodeposition, ensuring the control of the sensor thickness, as well as its reproducibility and stability. The characterization was performed using atomic force microscopy (AFM), scanning electron microscopy (SEM), electrochemical impedance spectroscopy (EIS) and X-ray Photoelectron Spectroscopy (XPS). The MIP/AuNP/RGO-GCE electrochemical sensor showed high sensitivity, selectivity, low detection limit, good stability and reproducibility. The sensor was successfully applied in the determination of D-mannitol in sugarcane vinasse.

## 2. Experimental

### 2.1. Reagents and apparatus

o-Phenylenediamine (purity:  $\geq 98\%$ ), D-mannitol (purity:  $\geq 98\%$ ), potassium ferricyanide ( $K_3[Fe(CN)_6]$ , purity: 99%), chloroauric acid and graphene oxide suspension (GO, purity:  $> 95\%$ ) were purchased from Sigma–Aldrich. Potassium chloride, potassium dihydrogen phosphate, dipotassium hydrogen phosphate, sodium acetate were employed as supporting electrolyte. Acetonitrile-acetic acid 5:2 (v/v) was used to extract the template from the MIP matrix. Stock solution of  $1.0 \times 10^{-2} \text{ mol L}^{-1}$  D-mannitol and o-PD were prepared in  $0.1 \text{ mol L}^{-1}$  acetate buffer solution under pH 5.0 for electropolymerization. The oxidation probe solution was  $5.0 \times 10^{-3} \text{ mol L}^{-1}$   $K_3Fe(CN)_6$  in  $0.1 \text{ mol L}^{-1}$  KCl. Phosphate buffer solution (PBS,  $0.1 \text{ mol L}^{-1}$ ) of pH 6.5 was used as the rebinding solution to D-mannitol. All the solutions were prepared with ultrapure water.

The electrochemical measurements were performed using a potentiostat Autolab PGSTAT30 coupled to a microcomputer that records and stores data obtained using the control software Nova 1.11. A conventional electrochemical cell with three electrodes, reference electrode Ag/AgCl ( $KCl$   $3.0 \text{ mol L}^{-1}$ ), platinum wire being auxiliary electrode and glassy carbon (diameter  $3.0 \text{ mm}$ ) as working electrode were used. A magnetic stirrer was used for the convective transport when necessary. All experiments were carried out at room temperature.

### 2.2. Cleaning procedure for GCE

The GCE electrode was polished with  $0.3 \mu\text{m}$  alumina powder on a felt and electrochemically polished by successive scans in potential range between  $-0.5$  and  $+1.5 \text{ V}$  in  $0.5 \text{ mol L}^{-1}$   $H_2SO_4$ , at  $20 \text{ mV s}^{-1}$ , until the voltammogram cyclic characteristics for a clean GCE were obtained.

### 2.3. Preparation of RGO-GCE

The reduced graphene oxide (RGO) film was prepared by electrodeposition of a suspension of graphene oxide (Sigma-Aldrich-USA), onto bare surface of GCE based on previous work [29,30]. Parameters such as graphene oxide suspension concentration, applied potential and deposition time were optimized as shown in Fig. S1 of the supplementary material, where  $0.5 \text{ mg mL}^{-1}$  of graphene oxide suspension in  $0.1 \text{ mol L}^{-1}$   $Na_2SO_4$  was electrodeposited at potential of  $-1.5 \text{ V}$  for 600 s. Following modification, the electrode was dried at room temperature.

### 2.4. Preparation of AuNP/RGO-GCE

The nanoparticles gold (AuNP) was electrodeposited on the surface of RGO/GCE film by chronoamperometry. The best results for electrodeposition of the AuNP were determined as  $+0.40 \text{ V}$  potential for 120 s in  $0.5 \text{ mol L}^{-1}$   $H_2SO_4$  solution containing  $6.0 \times 10^{-4} \text{ mol L}^{-1}$   $HAuCl_4$ . All the parameters that affect the formation of the modified electrode, such as concentration, deposition time and potential are shown in Fig. S2 of the supplementary material.

## 2.5. Preparation of the MIP in AuNP/RGO-GCE

Electropolymerization of the MIP was performed by cyclic voltammetry (CV) on the AuNP/RGO-GCE, between  $-0.4$  and  $+1.0$  V for 27 consecutive cycles at a scan rate of  $50 \text{ mV s}^{-1}$  in  $0.1 \text{ mol L}^{-1}$  acetate buffer solution under pH 5.0, containing  $3.0 \times 10^{-4} \text{ mol L}^{-1}$  D-mannitol and  $5.0 \times 10^{-4} \text{ mol L}^{-1}$  o-PD as a functional monomer. After electropolymerization the electrode was soaked in acetate buffer solution of pH 5.0 to remove non-polymeric o-PD from the electrode surface. To remove the D-mannitol template, the MIP electrode was washed with acetonitrile-acetic acid 5:2 (v/v) for 60 s at room temperature, under stirring. For comparison and control, a non-imprinted polymer (NIP/AuNP/RGO-GCE) was made following the same procedure, but without adding D-mannitol to check the reliability of the measurements. All optimizations and discussion of each parameter are in the SI.

## 2.6. Electroanalytical measurements

Upon the extraction of the D-mannitol molecules, the electrode was rinsed thoroughly with ultra-pure water and then subjected to rebinding and selective recognition experiments. Rebinding of D-mannitol in the cavities formed was carried out through the immersion of the electrode in different concentration of D-mannitol solutions in  $10 \text{ mL}$  of  $0.1 \text{ mol L}^{-1}$  PBS (pH 6.5) under stirring for 15 min, followed by the careful washing of the electrode with distilled water to remove the adsorbed physical substances. The electrode was subsequently placed in a three-electrode conventional cell with MIP/AuNP/RGO-GCE as working electrode. The solution of  $5.0 \times 10^{-3} \text{ mol L}^{-1}$   $[\text{Fe}(\text{CN})_6]^{3-/4-}$  in  $0.1 \text{ mol L}^{-1}$  KCl was chosen as an electrochemical active probe to study the performances of the prepared sensor. Imprinted cavities formed can provide a pathway for the diffusion of the probe through the MIP matrix. The probe can then be oxidized or reduced on the electrode, producing an electrochemical signal proportional to the number of cavities that have not been occupied by the D-mannitol molecule. By so doing, the cyclic voltammetry (CV) was recorded at potentials ranging between  $-0.2$  and  $+0.6$  V at a scan rate of  $10 \text{ mV s}^{-1}$ . Differential pulse voltammograms (DPV) were recorded by scanning at the potential range of  $-0.2$  to  $+0.5$  V at modulation amplitude of  $50 \text{ mV}$ , modulation time of  $50 \text{ ms}$  and step potential of  $4.0 \text{ mV}$ . The unknown concentrations of D-mannitol were determined by the standard addition method. All measurements were performed at room temperature.

The figures of merit such as limit of detection (LOD), limit of quantification (LOQ) and amperometric sensitivity (As) were determined. LOD and LOQ were calculated according to the equation  $\text{LOD} = 3.3 \text{ SD/S}$  and  $\text{LOQ} = 10 \text{ SD/S}$  where SD is the standard deviation of the intercept, and S being the slope of the calibration curve.

## 2.7. Characterizing the electrochemical sensor

For the purpose of characterizing the electrochemical sensor, electrochemical impedance spectroscopy (EIS) was carried out at a potential of  $0.22 \text{ V}$  over the frequency range of  $0.1 \text{ Hz}$  to  $100 \text{ kHz}$ . To study the morphology of the original surface, scanning electron microscope with field emission gun (SEM-FEG) of Jeol, model JSM 7500 F was used. Furthermore, atomic force microscopy (AFM) in tapping mode was used (Bruker nonoscope V). The modified surfaces were analyzed on a sample holder of  $2.0 \mu\text{m} \times 2.0 \mu\text{m}$  and the sample area was displayed with a  $256 \times 256$  pixels resolution. The scan rate was  $2.0 \mu\text{m s}^{-1}$ . A commercial spectrometer (UNI-SPECS UHV) was employed at a pressure below  $10^{-7} \text{ Pa}$ , for the XPS analysis. The Mg K $\alpha$  line was used ( $h\nu = 1253.6 \text{ eV}$ ) while the analyzer pass energy was set to  $10 \text{ eV}$ . The inelastic background of Au 4f, N 1s, O 1s and C 1s electron core-level spectra was subtracted using Shirley's method. The composition (at.%) of the near surface region was determined with an accuracy of  $\pm 10\%$  from the ratio of the relative peak areas corrected by Scofield's sensitivity factors of the corresponding elements. The C 1s

hydrocarbon component of the fixed value of  $285.0 \text{ eV}$  was used for correcting the binding energy scale of the spectra. The spectra were fitted without placing constraints using multiple Voigt profiles. The width at half maximum (FWHM) varied between  $1.2$  and  $2.1 \text{ eV}$  and the accuracy of the peak positions was  $\pm 0.1 \text{ eV}$ .

## 2.8. D-mannitol detection in sugarcane vinasse sample

The vinasse was centrifuged to remove the solid particles at  $4000 \text{ rpm}$  for  $20 \text{ min}$  while the supernatant was collected and filtered using filters with porosity of  $0.47$  and  $0.22 \mu\text{m}$ . The sample was diluted  $2000$  times in  $0.1 \text{ mol L}^{-1}$  PBS (pH 6.5) and used for D-mannitol detection. The same procedure was adopted for the recovery experiment where known amounts of standard D-mannitol were added to the samples.

## 3. Results and discussion

### 3.1. Preparation and electrochemical characterization of MIP/AuNP/RGO-GCE

CV and EIS techniques were used for monitoring the electrochemical properties of each step of the electrode modification. Considering that D-mannitol is not an electroactive compound in the pH range necessary to maintain the proper functioning of the MIP [29], in this work, we used the solution containing  $5.0 \times 10^{-3} \text{ mol L}^{-1}$   $[\text{Fe}(\text{CN})_6]^{3-/4-}$  in  $0.1 \text{ mol L}^{-1}$  KCl as electrochemical probe to monitor the change of the electrochemical behavior during the formation of the sensor. A couple of typical redox peaks was observed on the bare glassy carbon electrode as shown in Fig. 1A (curve a). After the GCE modification with RGO (curve b), the peak currents increased as a result of better electrical conductivity and high surface-to-volume ratio of the graphene nanosheets. Interestingly, when the RGO-GCE electrode was modified with AuNP (curve c), the current was found to increase at an even higher degree. The reason for this higher increase in current response is attributed to the size of the gold nanoparticles which tends to contribute towards enabling the occurrence of the electron transfer in a much easier way through the electrochemical probe [30] while consequently rendering the sensor more sensitive.

On the AuNP/RGO-GCE electrode, a thin film of o-PD was electropolymerized by consecutive cyclic scans until the gradual covering of the electrode, leading to the restraint of the voltammetric response, as displayed in Fig. S3 in the supplementary material. In the first scan, an irreversible anodic oxidation peak appeared at a potential of  $+0.4 \text{ V}$  relating to the oxidation of the o-PD to the dimer state [31]. It is worth noting that a drop in current is seen in the sequential cycles, indicating the formation of a non-conductive film on the electrode surface. No notable differences were observed between the electropolymerization in the presence and absence of D-mannitol, which demonstrates that the molecule does not undergo any electrochemical oxidation and reduction under the potential range of electropolymerization. During the electropolymerization, the D-mannitol molecules were seen trapped in the polymer matrix which can be attributed to the ability of these molecules to interact with the units of o-PD. The hydrogen bonding may occur between the hydrogen of the hydroxyl group of D-mannitol structure with the nitrogen atom of the N-H group of o-PD units. This process is capable of generating cavities with shape and position of the functional groups which makes the selective recognition of D-mannitol possible.

In Fig. 1B, no peak is observed on the MIP and NIP electrodes prior to the template removal (curves d and e), this can be explained by the compact and non-conductive film electropolymerized on the surface. Following the removal of D-mannitol molecules using acetonitrile/acetic acid in the ratio 5:2 (v/v), there was a rupture of the hydrogen bonds between the functional monomers and the template molecules along with the formation of imprinted cavities in the MIP, where a

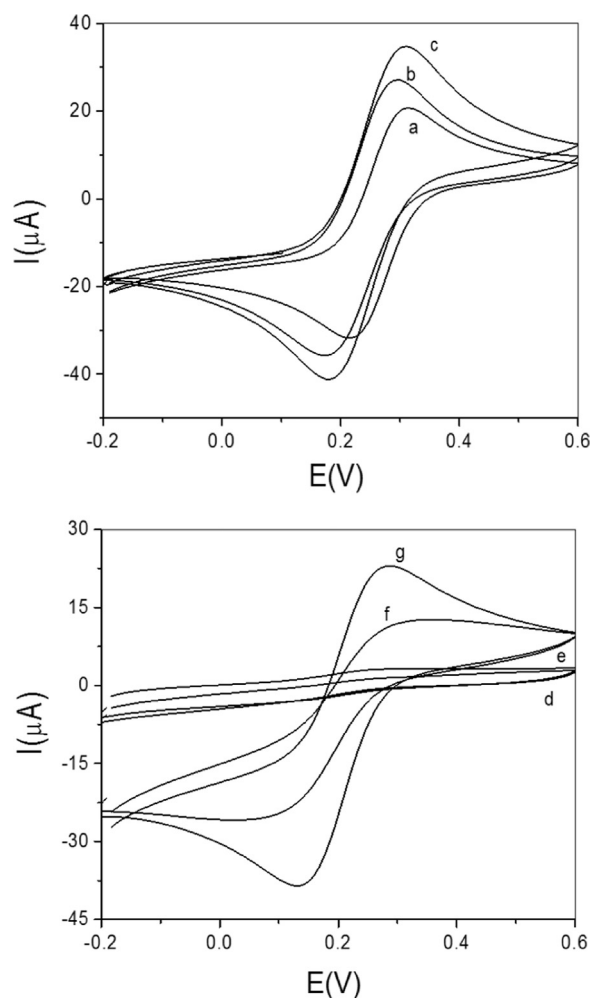


**Fig. 1.** In the lower left corner: CV of (a) bare GCE (b) RGO-GCE and (c) AuNP/RGO-GCE. (d) MIP (e) NIP (f) MIP after template of D-mannitol and (g) MIP after rebinding  $5.0 \times 10^{-12}$  mol L $^{-1}$  D-mannitol, in solution containing  $5.0 \times 10^{-3}$  mol L $^{-1}$  [Fe(CN) $_6$ ] $^{3-/4-}$  in 0.1 mol L $^{-1}$  KCl.

couple of redox peaks could be observed (curve g), demonstrating that some channels were created and that the probe ions are able to pass through the cavities to the AuNP/RGO surface. Furthermore, after the immersion of the MIP/AuNP/RGO-GCE in 0.1 mol L $^{-1}$  PBS (pH 6.5) containing  $5.0 \times 10^{-12}$  mol L $^{-1}$  of D-mannitol for 15 min, the peak current was found to decrease (curve f), which reveals that some cavities were combined again with D-mannitol, blocking the arrival of the probe to the electrode surface, thus confirming the existence of imprinted sites on the MIP. In order to confirm whether D-mannitol has been embedded on the o-PD film, the electrode was electropolymerized in the presence (MIP) and absence of D-mannitol (NIP).

EIS was used for the characterization of the modified electrode. The electron-transfer resistance was investigated using a solution of  $5.0 \times 10^{-3}$  mol L $^{-1}$  [Fe(CN) $_6$ ] $^{3-/4-}$  in 0.1 mol L $^{-1}$  KCl as redox probe (Fig. 2). The typical shape of EIS includes a semicircle and a straight line. A circuit compatible with the Nyquist diagram is shown in Fig. 2. In this circuit,  $R_s$  stands for the solution resistance, CPE being the constant phase element which is related to the double layer capacitance,  $R_{ct}$  representing the charge-transfer resistance. The data were discussed in terms of  $R_{ct}$  for the fact that it has a simple physical meaning when compared to the other elements, and describes the rate of charge transfer during the electrode reaction [31].

At the upper right hand side of Fig. 2, one can see the EIS of (a) bare GCE, (b) RGO-GCE and (c) AuNP/RGO-GCE. It can be observed that a well-defined semicircle was obtained on the bare GCE while a decrease in resistance was seen for the RGO-GCE and AuNP/RGO-GCE

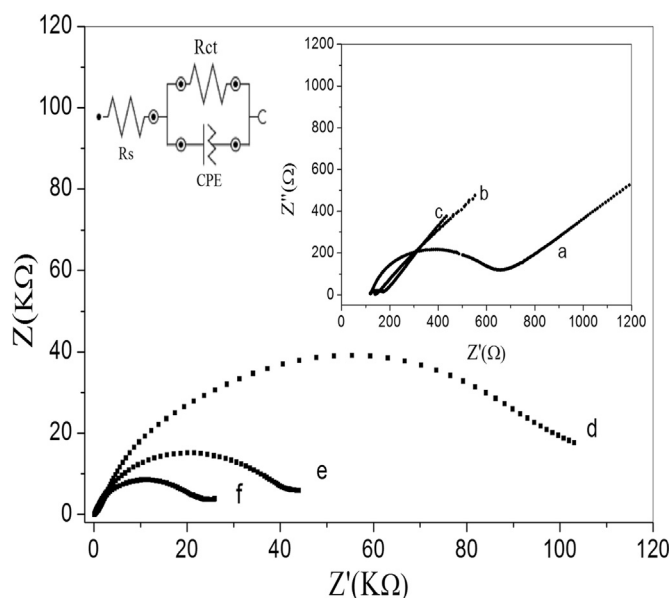


**Fig. 2.** Nyquist diagrams of EIS of different electrodes (a) bare GCE (b) RGO-GCE (c) AuNP/RGO-GCE (d) MIP/AuNP/RGO-GCE before extraction of D-mannitol (e) MIP/AuNP/RGO-GCE after rebinding of D-mannitol (f) MIP/AuNP/RGO-GCE after extraction of D-mannitol. The supporting solution contained  $5.0 \times 10^{-3}$  mol L $^{-1}$  [Fe(CN) $_6$ ] $^{3-/4-}$  and 0.1 mol L $^{-1}$  KCl and the frequency range was of 0.01 Hz to 100 kHz.

(curves b and c), with the  $R_{ct}$  values for GCE, RGO-GCE, and AuNP/RGO-GCE being about 547  $\Omega$ , 76.72  $\Omega$  and 25  $\Omega$  respectively, indicating that the modification may facilitate the transfer of electrons. The increase observed in the  $R_{ct}$  for the MIP/AuNP/RGO-GCE (curve d) layer could be a consequence of the resistance of compact and nonconductive o-PD film at the electrode/solution interface. However, in curve f, the  $R_{ct}$  is found to undergo a remarkable decrease after the removal of D-mannitol, suggesting the successful formation of cavities following the extraction of D-mannitol molecules, and thus leaving channels for the penetration of [Fe(CN) $_6$ ] $^{3-/4-}$ . In curve e, an increase is seen in the  $R_{ct}$ , which can be attributed to the rebinding of the D-mannitol into the imprinted cavities again, blocking the arrival of the probe onto the electrode surface.

### 3.2. Surface topographical characterization of the imprinted sensor

The surface morphological analysis was investigated by atomic force microscope (AFM) and scanning electron microscope (SEM). The AFM 3D is shown in Fig. 3. In Fig. 3a, we can observe that the electrode was homogeneously modified by AuNP/RGO, with nanoparticles having an average of 80 nm of diameter and 40 nm of height, with roughness of 16.6 nm, expressed in terms of the root-mean-square (RMS) value (RMS is proportional to roughness). A marked change in roughness is evident when modifying the electrode with the polymeric film during the molecular imprinting process. The RMS values obtained were 52.4 nm for MIP prior to the removal of the D-mannitol molecule (Fig. 3b) and 23.7 nm for MIP after the removal (Fig. 3c) of the molecule. This difference shows that the electrodeposition of o-PD along with the removal of D-mannitol were both successfully performed. The RMS value for NIP was 19.6 nm, showing that the film was relatively flat and compact (Fig. 3c).

Furthermore, SEM images were analyzed as shown in the supplementary material. Fig. S4A and B exhibit SEM images of RGO-GCE and AuNP/RGO-GCE respectively. The images show the uniform electrodeposition of AuNP on the graphene nanosheets with a homogeneous distribution on the glassy carbon surface. As can be seen in Fig. S4C and D, the formation of MIP on the AuNP/RGO-GCE presented a relatively more wrinkled surface compared to NIP (Fig. S4E) which exhibited a smoother and less wrinkled surface. The Fig. S4F represents



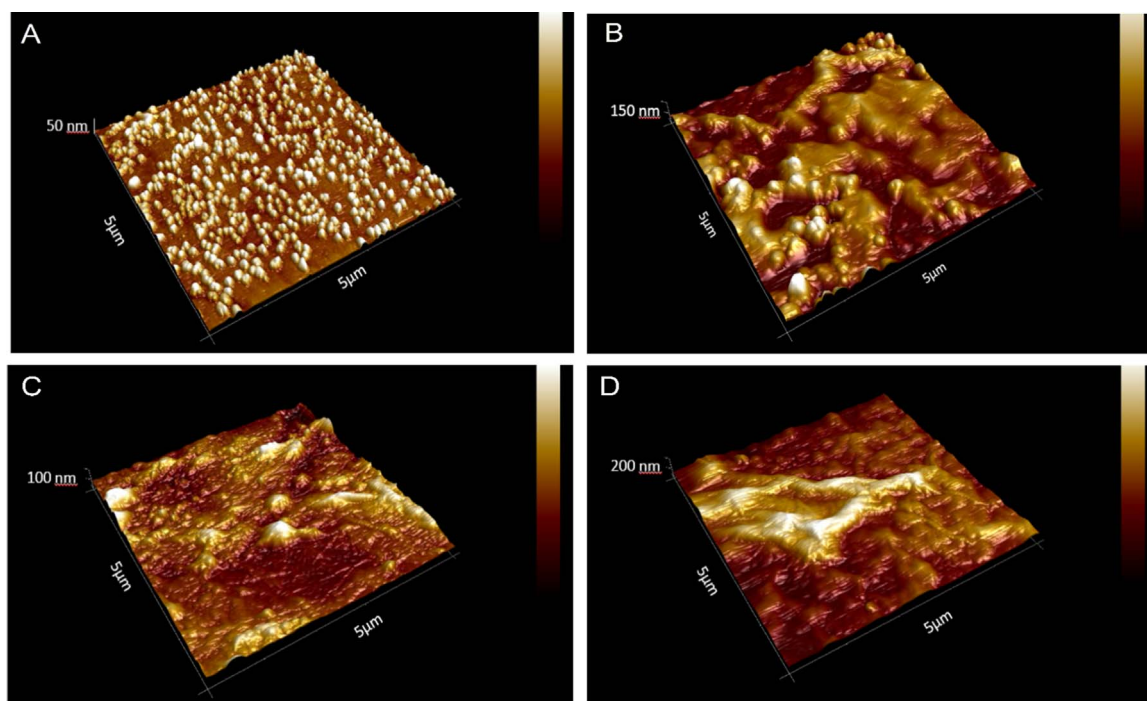


Fig. 3. AFM images, (a) AuNP/RGO-GCE electrode, (b) MIP before template removal, (c) MIP after template removal and (d) NIP.

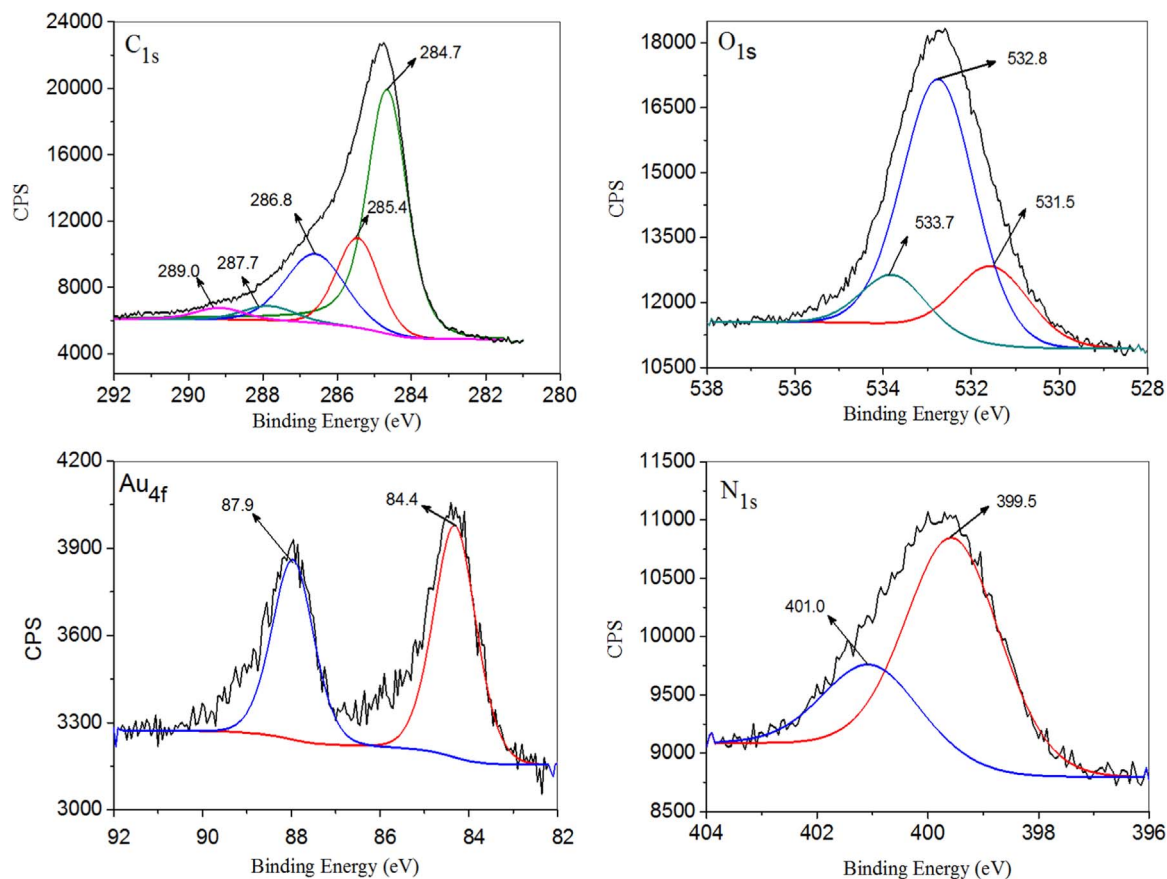


Fig. 4. Deconvoluted C1s, O1s, Au4f and N1s XPS spectrum of the MIP/AuNP/RGO-GCE.

the respective EDX for AuNP/RGO-GCE.

The surface chemistry of MIP/AuNP/RGO-GCE was also characterized using XPS in order to investigate the oxidation level as well as the nature of the chemical bonding (Fig. 4).

The high-resolution C1s spectra of the samples can be deconvoluted into five components corresponding to carbon atoms in different functional groups with binding energies (BE) 284.7 (C-H), 285.4 (C-N), 286.8 (C-O), 287.7 (C=O) and 289.0 (O-C=O) eV [32]. The oxygen

content was monitored by the O1s signal. The high-resolution O1s spectra of the samples can be deconvoluted into three components corresponding to oxygen atoms in different functional groups at 531.5 (C=O), 532.8 (C-O) and 533.7 (O-C=O) eV, attesting to the fact that the electrode was functionalized with RGO. The Au4f<sub>7/2</sub> peak at 83.1 eV confirms the presence of Au on the surface. The signal at 87.9 eV can be attributed to the gold nanoparticles that did not undergo electrical reaction. The XPS spectra of N1s was deconvoluted into two components. The peak observed at 399.5 eV corresponds to the N–H groups of amide while that of the unreacted N–H groups is seen at 401.0 eV [33]. XPS wide spectra were also obtained as shown in Fig. S5. As can be clearly noted, when compared with AuNP/RGO-GCE (Fig. S5A), MIP/AuNP/RGO-GCE (Fig. S5B) exhibits an N1s signal, which emerged, probably, as a result of the nitrogen contained in the o-PD. Therefore, combining the SEM, EDX, AFM and XPS results, we can fairly deduce that reduced graphene oxide, gold nanoparticles and o-PD polymer layer were successfully formed on the electrode surface.

### 3.3. Optimization of the preparation conditions for MIPs

A thorough study was conducted regarding the effects of several parameters including the concentration of monomer and template, number of electropolymerization cycles, pH of the electropolymerization solution, template extraction, extraction time and rebinding of the D-mannitol in the specific cavities aiming at developing an efficient sensor and obtaining the best performance. All the parameters enable us to determine the thickness likewise the physical stability of the polymer film besides the quality of the cavities formed. All the optimization experiments were performed using DPV to obtain the best conditions for the formation of the MIP while the change of current [Fe(CN)<sub>6</sub>]<sup>3-/4-</sup> ( $\Delta I$ ) was used to evaluate the optimum condition. Each of these parameters is deemed essentially crucial for the good performance of the sensor, as such they are discussed below.

#### 3.3.1. Number of cycles for electropolymerization

The number of cycles was found to directly affect the sensor sensitivity and was evaluated by the comparison between the MIP and the NIP electrode responses. As can be seen in Fig. S6, a considerable decrease was found in the performance of the MIP below 20 cycles while the formation of a very thick film occurred over 30 cycles, impeding the probe from getting into some cavities situated in the middle, thus increasing the mass-transfer resistance. Thick films demonstrated poor accessibility, resulting in the loss of sensor sensitivity. The best condition was thus obtained through the application of 27 cycles.

#### 3.3.2. Effect of pH in electropolymerization

Another factor that influences the formation of MIP is the pH. Fig. S7 shows the dependence of the peak current in the pH range of 4.8 to 5.4. This pH range was chosen owing to the fact that at a more acidic pH the amino groups of the o-PD unit are condensed with the adjacent benzene ring along the polymer chain (although this structure also has free NH<sub>2</sub> groups). At high pH levels, the extent of conjugation is gradually decreased due to the increase of free NH<sub>2</sub> groups. The ability of the o-PD polymerizing and interacting with the template molecule is around pH 5.0. In this case, the presence of neutral or protonated NH<sub>2</sub> may be responsible for the interaction with D-mannitol used as template.

#### 3.3.3. Effect of the monomer concentration

The concentration of monomer during the electropolymerization process directly affects the thickness of the film and is related to the sensitivity. In order to study the effect the monomer concentration had on the sensor response, the concentration of o-PD was studied in the range of  $2.0 \times 10^{-4}$  mol L<sup>-1</sup> to  $1.2 \times 10^{-3}$  mol L<sup>-1</sup>, as shown in Fig. S8. In concentrations inferior to  $4.0 \times 10^{-4}$  mol L<sup>-1</sup> o-PD, the MIP was found

to be less sensitive, probably due to the fact that the D-mannitol molecules are incapable of being trapped in considerable quantities during the electropolymerization process. Nonetheless, high concentrations of o-PD are likely to lead to non-selectivity of the electrochemical response, owing to the fact that the greater thickness of the film causes difficulty in the removal of the template. Hence,  $5.0 \times 10^{-4}$  mol L<sup>-1</sup> of o-PD monomer was chosen aiming at obtaining the highest sensitivity.

#### 3.3.4. Effect of the template concentration

The D-mannitol concentration in the polymerization solution is found to exert an influence on the amount of recognition cavities available for the selective rebinding of the template. Fig. S9 shows the effect of different concentrations of the D-mannitol ( $7.5 \times 10^{-5}$  mol L<sup>-1</sup> to  $7.5 \times 10^{-4}$  mol L<sup>-1</sup>) on the MIP response during the electropolymerization process. It was observed that the largest  $\Delta I$  was obtained when the template concentration was  $3.0 \times 10^{-4}$  mol L<sup>-1</sup>. When the amount of D-mannitol was below  $3.0 \times 10^{-4}$  mol L<sup>-1</sup>, the MIP response was found to decrease, which can certainly be associated with the lower number of imprinted cavities and consequently lesser sensitivity. The sensor prepared in a higher concentration of D-mannitol also showed poor sensitivity. This could be attributed to the increase in agglomeration of the molecules, creating larger cavities with loss of selectivity. Therefore, the optimum template concentration was found to be  $3.0 \times 10^{-4}$  mol L<sup>-1</sup>.

#### 3.3.5. Template removal

With the purpose of using the imprinted sensor in the voltammetric analysis, it becomes necessary to remove the template molecule, so as to form the recognition cavities. The removal of the D-mannitol molecules from the polymer chain for the cavities generation must be complete in order to ensure good reproducibility and sensitivity of the sensor. Alcohol, ultrapure water, NaOH solution, methanol/acetic acid, methanol/water, acetonitrile/water, ethanol/water, acetonitrile/acetic acid were used respectively for the selective formation of cavities. The results indicated that acetonitrile/acetic acid quickly and completely removed the template molecule when used in the ratio 5:2 (v/v). The removal occurs as a result of the affinity of the solvent to the polymer. The molecules of the solvent penetrate the polymeric mass moving away segments of the chains, promoting swelling of the polymer and the release of the template molecule by virtue of the weakening of the hydrogen bonds between the polymer and the template molecule. Fig. S10 shows the variation of the current ( $\Delta I$ ) at different extraction times (30 s to 90 s). As can be seen, the current rapidly increases with an increase in the immersion time, though it is found to decline gradually after immersion time above 60 s. At 90 s, the electrode is found to present no significant current, indicating that the swelling of the polymer blocked the whole of the electroactive surface. Thus, the electrode immersion in acetonitrile/acetic acid solution in the ratio 5:1 (v/v) for 60 s was chosen as the best condition for the removal of the template.

#### 3.3.6. Rebinding of the molecule

The influence of rebinding time on the MIP response was investigated. Following the template removal, the electrode was placed in 0.1 mol L<sup>-1</sup> PBS (pH 6.5) containing  $5.0 \times 10^{-12}$  mol L<sup>-1</sup> of D-mannitol, under stirring for a certain time interval. Fig. S11 shows the effect of rebinding time on the MIP response. The results showed that there was an increase in response relative to the rebinding time. A stable response was obtained after 15 min, suggesting that the adsorption equilibrium was achieved. As a result, the rebinding time of 15 min was selected for subsequent studies.

In short, the optimized experimental conditions included the following: The electropolymerization was carried out within the potential range of -0.4 to 1.0 V for 27 cycles in acetate buffer under pH 5.0. The results obtained relating to the amount of monomer and template were  $5.0 \times 10^{-4}$  mol L<sup>-1</sup> and  $3.0 \times 10^{-4}$  mol L<sup>-1</sup>, respectively.

The best extraction time was found to be at 60 s in the acetonitrile and acetic acid solution in the ratio 5:2 (v/v), being the conditions under which the template can be removed in a quick and efficient manner. D-mannitol rebinding in the formed cavities occurred in 15 min in PBS under pH 6.5.

### 3.4. Electrochemical behavior of the electrochemical active probe

Cyclic voltammetry is an important tool for the mechanistic and kinetic studies of redox reactions that occur on the electrode surface [34]. The electrochemical mechanism was investigated based on the relationship between the peak current and the scan rate in  $5.0 \times 10^{-3} \text{ mol L}^{-1} [\text{Fe}(\text{CN})_6]^{3-/4-}$  solution on the electrode modified with MIP/AuNP/RGO-GCE in the range of 10 to  $100 \text{ mV s}^{-1}$  scan rate. The peak currents of the CV on the imprinted electrode were found to increase given an increase in the scan rate (Fig. S12). The  $I_{pa}$  and  $I_{pc}$  showed a linear dependence relationship with the root of the speed and can be expressed as:  $I_{pa} (\mu\text{A}) = 0.63 v^{1/2} + 4.07$  ( $R = 0.998$ ) and  $I_{pc} (\mu\text{A}) = -0.62 v^{1/2} - 4.18$  ( $R = 0.997$ ), indicating a mass diffusion-controlled process, which is the ideal case for quantitative determination [35].

### 3.5. Analytical performance

Under the optimum conditions, Fig. 5 shows the MIP/AuNP/RGO-GCE sensor response in DPV after rebinding of varying concentrations of D-mannitol and the corresponding cyclic voltammograms. The peak current was found to decrease as the D-mannitol concentration increased, this can be said to be as a result of the occupation of the cavity sites in the MIP film by D-mannitol molecules. Accordingly, the reduction in  $\Delta I$  for  $[\text{Fe}(\text{CN})_6]^{3-/4-}$  was proportional to the D-mannitol concentration in two linear ranges:  $1.0 \times 10^{-12}$  to  $2.0 \times 10^{-11} \text{ mol L}^{-1}$  and  $2.0 \times 10^{-11}$  to  $3.0 \times 10^{-10} \text{ mol L}^{-1}$ . The first linear range was used to obtain the figures of merit. The linear regression equation was  $\Delta I (\mu\text{A}) = 3.9 \times 10^{10} C_{\text{D-mannitol}} + 0.2$  with a correlation coefficient of 0.998, with LOD of  $7.7 \times 10^{-13} \text{ mol L}^{-1}$ , LOQ of  $2.6 \times 10^{-12} \text{ mol L}^{-1}$  and amperometric sensitivity (As) of  $3.9 \times 10^{10} \mu\text{A L mol}^{-1}$ , ( $n=3$ ).

In Table 1, the results obtained for the MIP sensor are compared with other reported electrochemical methods where the proposed sensor is seen to exhibit a lower detection limit.

The presence of two linear ranges in the MIP sensor can be

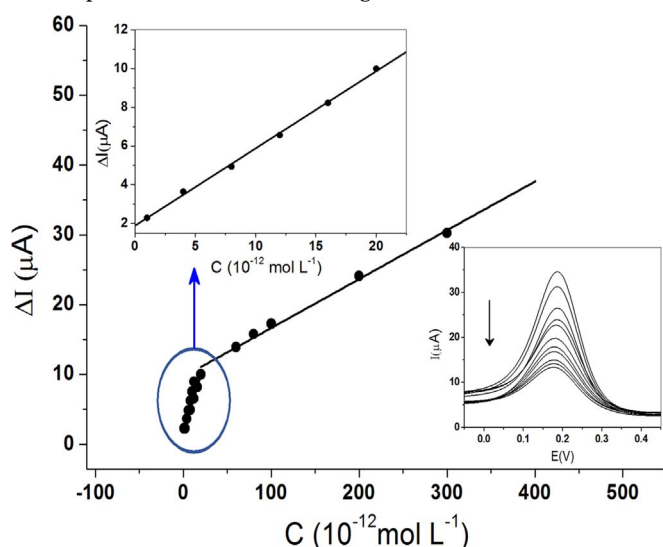


**Fig. 5.** Calibration curves for D-mannitol detection using MIP/AuNP/RGO-GCE in  $5.0 \times 10^{-3} \text{ mol L}^{-1} [\text{Fe}(\text{CN})_6]^{3-/4-}$  after 15 min of rebinding in PBS under pH 6.5. The curve presented in the top-left inset is obtained with the D-mannitol concentration in the range of  $1.0 \times 10^{-12}$  to  $2.0 \times 10^{-11} \text{ mol L}^{-1}$ . Differential pulse voltammograms in accordance with D-mannitol concentration in the range of  $1.0 \times 10^{-12}$  to  $3.0 \times 10^{-10} \text{ mol L}^{-1}$  are in the bottom-left inset.

explained by the different levels of affinity between the imprinted sites and D-mannitol molecules. In this sense, when D-mannitol is at low concentration, the molecules prefer to occupy the imprinted sites of high affinity, located on the surface of the MIP sensor. The low-affinity sites located more deeply are occupied when there are large quantities of D-mannitol molecules, causing a decline in slope in the linear regression equation.

The reproducibility of the imprinted sensor was investigated prior to and after rebinding in  $5.0 \times 10^{-12} \text{ mol L}^{-1}$  D-mannitol solution in five different sensors prepared independently under the same conditions (each electrode was carried out in three replications). The relative standard deviation (RSD) was 3.4%. Repeatability was evaluated for three successive times with the same modified electrode. The RSD was 1.9%. The stability of the MIP sensor was measured after having been stored for 20 days dry and at room temperature ( $25^\circ\text{C}$ ). The results showed that the sensor still presented 91.7% of its initial current after this period, demonstrating that it, indeed, has good stability. The sensor can be reused by approximately 45 times. The results clearly indicate that MIP/AuNP/RGO-GCE possesses good repeatability, reproducibility and stability, thus suggesting the suitability nature of the proposed method when it comes to D-mannitol analysis.

The selectivity of the MIP/AuNP/RGO-GCE sensor was evaluated comparing DPV responses to D-mannitol along with some possible interfering molecules that have similar structure including myo-inositol, L-arabitol, glycerol (the same class as the D-mannitol), in addition to sucrose and glucose, which are carbohydrates that can interfere in the analysis. Two factors are known to play key roles in selectivity: the functional groups of the molecules and their size. Molecules containing the same functional group and being of the same size are found to have more interfering effect [31]. The change of current response of  $[\text{Fe}(\text{CN})_6]^{3-/4-}$  in the MIP sensor at the same concentration ( $5.0 \times 10^{-12} \text{ mol L}^{-1}$ ) of each molecule was analyzed using DPV.

As can be observed in Fig. 6, L-arabitol and glycerol present a slight interference which can be attributed to the fact that these compounds are smaller in size compared to the D-mannitol molecule occupying the imprinting sites. Sucrose is found to be larger in size compared to D-mannitol and as such is incapable of entering the imprinting cavities, the reason behind the observed slightest interference of this molecule. Molecules with different structures, such as myo-inositol, are more difficult to adhere to the printing sites largely due to steric hindrance.

In order to analyze the specificity and selectivity of the MIP sensor, the factor  $\alpha$  (imprinted) and  $\beta$  (selectivity) were defined to evaluate these parameters. The results are summarized in Table 2. The imprinted factor ( $\alpha$ ) showed greater response to the D-mannitol molecule compared to the interfering molecules, suggesting that the sensor has a special recognition and selectivity for D-mannitol owing to the imprinting effect. Analyzing the values for the selectivity factor ( $\beta$ ), the sensor was found to present more selectivity for the D-mannitol in comparison with the other molecules. These results suggest that the size as well as the conformation of the cavities for the MIP sensor was formed specifically to be selective in relation to the D-mannitol.

### 3.6. Determination of D-mannitol in sugarcane vinasse samples

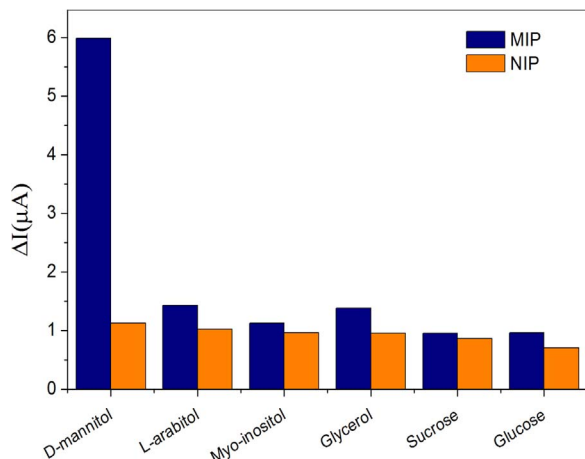
The standard addition method was used to determine the concentration of D-mannitol present in vinasse sample which consists of adding known concentrations of the substance of interest in the sample. In this work, the concentration of D-mannitol was in the range of  $2.0 \times 10^{-12}$  to  $6.0 \times 10^{-12} \text{ mol L}^{-1}$ . The samples were prepared as described in Section 2.5. All measurements were accomplished in triplicate with different electrodes. The samples were measured by DPV and the results are presented in Table 3. The concentration of  $0.19 \pm 0.05 \text{ mg}$  was found for D-mannitol per liter of vinasse.

The production of ethanol for 2016/2017, in Brazil, is estimated to be around 30.3 billion liters [36], which will produce nearly 454.4 billion liters of vinasse. If D-mannitol is to be recovered in a biorefinery

**Table 1**

Comparison of the linear range and detection limit for some reported methods used in electrochemical determination of D-mannitol.

Electrode	Linear Range (mol L <sup>-1</sup> )	Detection limit (mol L <sup>-1</sup> )	References
Au	$3.8 \times 10^{-7}$ – $5.0 \times 10^{-2}$	$3.8 \times 10^{-7}$	[9]
G/CuNP/CPE <sup>a</sup>	$1.0 \times 10^{-6}$ – $2.0 \times 10^{-3}$	$2.9 \times 10^{-7}$	[14]
CNT-CuNP hybrid paste electrode <sup>b</sup>	$1.0 \times 10^{-6}$ – $2.0 \times 10^{-3}$	$1.8 \times 10^{-7}$	[37]
Cu <sub>2</sub> O-CCE <sup>c</sup>	$8.0 \times 10^{-7}$ – $8.0 \times 10^{-4}$	$8.0 \times 10^{-7}$	[38]
Ni-CME <sup>d</sup>	$5.4 \times 10^{-6}$ – $1.1 \times 10^{-3}$	$2.7 \times 10^{-6}$	[39]
Au	$1.2 \times 10^{-8}$ – $1.1 \times 10^{-6}$	$5.1 \times 10^{-8}$	[40]
MIP/AuNP/RGO-GCE	$1.0 \times 10^{-12}$ – $2.0 \times 10^{-11}$	$7.7 \times 10^{-13}$	This Work

<sup>a</sup> graphene-copper nanoparticle composite paste electrode.<sup>b</sup> CNT refers to carbon nanotube and CuNP refers to copper nanoparticles.<sup>c</sup> CCE refers to carbon composite electrodes.<sup>d</sup> refers to chemically modified electrodes.**Fig. 6.** Selectivity comparison between the MIP and NIP sensors. Concentration of  $5.0 \times 10^{-12}$  mol L<sup>-1</sup> in PBS pH 6.5 for each molecule analyzed (rebinding time: 15 min). Response obtained in DPV for solution contained  $5.0 \times 10^{-3}$  mol L<sup>-1</sup> [Fe(CN)<sub>6</sub>]<sup>3-/4-</sup> in 0.1 mol L<sup>-1</sup> KCl.**Table 2**

Selectivity of MIP/AuNP/RGO/GCE for D-mannitol and interfering molecules.

Molecule	MIP (μA)	NIP (μA)	α <sup>a</sup>	β <sup>b</sup>
D-mannitol	29.9	6.1	4.9	1.0
L-arabitol	9.0	5.8	1.5	3.1
Myo-inositol	6.7	5.1	1.3	3.6
Glycerol	9.3	5.1	1.8	2.6
Sucrose	5.7	4.0	1.4	3.4
Glucose	5.8	5.1	1.1	4.2

<sup>a</sup>  $\alpha = (\Delta I_{\text{MIP}}) / (\Delta I_{\text{NIP}})$ .<sup>b</sup>  $\beta = (\alpha_{\text{D-mannitol}} / \alpha_{\text{interferent}})$ .**Table 3**

Determination of D-mannitol in sugarcane vinasse samples (n=3).

Sample	Amount added ( $10^{-12}$ mol L <sup>-1</sup> )	Amount detected ( $10^{-12}$ mol L <sup>-1</sup> )	Recovery (%)	RSD (%)
Vinasse	-	$5.2 \pm 0.5$	-	-
	2.0	$7.3 \pm 0.3$	100.9	4.5
	4.0	$8.9 \pm 0.2$	97.1	2.2
	6.0	$11.1 \pm 0.2$	99.4	1.4

from the sugarcane vinasse, an amount of 86.3 t would be available for use in the food and/or pharmaceutical industries.

The recoveries in standard solutions ranged from 97.1% to 100.9%, which indicates that the method has a relatively good degree of accuracy. Judging by the data presented, the MIP sensor can be

successfully applied towards the determination of D-mannitol in complex samples such as sugarcane vinasse.

#### 4. Conclusion

In this study, a novel sensor for the determination of D-mannitol was developed based on molecularly imprinted polymer on electrode modified with reduced graphene oxide and gold nanoparticles. The reduced graphene oxide combined with the gold nanoparticles were found to play a key role in improving the sensor performance which may be attributed to the increase in the conductive surface area, which has, in turn, contributed towards enhancing the electron transport and elevating the D-mannitol molecule immobilization sites per unit surface area, thereby leading to the prominent improvement of the selectivity and sensitivity of the sensor. The MIP/AuNP/RGO-GCE showed low detection limit and quantification, good repeatability and stability for up to 20 days when stored, besides its ability to be reused by approximately 45 times. The high recovery (between 97.1% and 100.9%) rate indicates that the proposed method has excellent degree of accuracy, being suitable for practical utility. In line with our expectations, the MIP sensor exhibited high selectivity to D-mannitol about six times greater compared to its counterpart. Moreover, the sensor has shown to be an excellent alternative for the determination of D-mannitol, even in samples containing similar molecules such as sugarcane vinasse.

#### Acknowledgment

The authors would like to express their sincerest gratitude and indebtedness to the Brazilian Research Funding Agencies – São Paulo Research Foundation (FAPESP) process n° 2014/23846-5 and Coordination for the Improvement of Higher Education Personnel (CAPES process n° 33004030072p8), for the financial support granted in the course of this research. Our thanks also go to the native English Language content editor – Brian Newmann for his painstaking editing and proofreading of the manuscript.

#### Appendix A. Supporting information

Supplementary data associated with this article can be found in the online version at doi:10.1016/j.talanta.2016.12.040.

#### References

- [1] P.S.M. de Oliveira, V.F. Ferreira, M.V.N. de Souza, E.M. de Carvalho, Síntese de aminoácidos derivados do D-manitol, Quim. Nova 31 (2008) 776–780.
- [2] J.S. Ko, J.E. Keum, S.Y. Ko, A synthesis of Oseltamivir (Tamiflu) starting from D-mannitol, J. Org. Chem. 75 (2010) 7006–7009.
- [3] J.P. Muizelaar, E.P. Wei, H.A. Kontos, D.P. Becker, Mannitol causes compensatory cerebral vasoconstriction and vasodilation in response to blood viscosity changes, J. Neurosurg. 59 (1983) 822–828.
- [4] M.D. Sorani, G.T. Manley, Dose–response relationship of mannitol and intracranial



- pressure: a metaanalysis, *J. Neurosurg.* 108 (2008) 80–87.
- [5] P.M. Medeiros, B.R.T. Simoneit, Analysis of sugars in environmental samples by gas chromatography-mass spectrometry, *J. Chromatogr. A* 1141 (2007) 271–278.
  - [6] I. Molnár-Perl, Simultaneous quantitation of acids and sugars by chromatography: gas or high-performance liquid chromatography, *J. Chromatogr. A* 845 (1999) 181–195.
  - [7] M.A. Cox, T.H. Iqbal, B.T. Cooper, K.O. Lewis, An analytical method for the quantitation of mannitol and disaccharides in serum: a potentially useful technique in measuring small intestinal permeability in vivo, *Clin. Chim. Acta* 263 (1997) 197–205.
  - [8] I.G. Casella, M. Gatta, E. Desimoni, Applications of a copper-modified gold electrode for amperometric detection of polar aliphatic compounds by anion-exchange chromatography, *J. Chromatogr. A* 814 (1998) 63–70.
  - [9] V.P. Hanko, J.S. Rohrer, Determination of carbohydrates, sugar alcohols, and glycols in cell cultures and fermentation broths using high-performance anion-exchange chromatography with pulsed amperometric detection, *Anal. Biochem.* 283 (2000) 192–199.
  - [10] S.C. Fleming, M.S. Kapembwa, M.F. Laker, G.E. Levin, G.E. Griffin, Rapid and simultaneous determination of lactulose and mannitol in urine, by HPLC with pulsed amperometric detection, for use in studies of intestinal permeability, *Clin. Chem.* 36 (1990) 797–799.
  - [11] R. Andersen, A. Sørensen, Separation and determination of alditols and sugars by high-pH anion-exchange chromatography with pulsed amperometric detection, *J. Chromatogr. A* 897 (2000) 195–204.
  - [12] Y. Xiao, Y. Li, J. Ying, Y. Tian, Y. Xiao, Z. Mei, Determination of alditols by capillary electrophoresis with indirect laser-induced fluorescence detection, *Food Chem.* 174 (2015) 233–239.
  - [13] P. Liang, M. Sun, P. He, L. Zhang, G. Chen, Determination of carbohydrates in honey and milk by capillary electrophoresis in combination with graphene-cobalt microsphere hybrid paste electrodes, *Food Chem.* 190 (2016) 64–70.
  - [14] Q. Chen, L. Zhang, G. Chen, Facile preparation of graphene-copper nanoparticle composite by in situ chemical reduction for electrochemical sensing of carbohydrates, *Anal. Chem.* 84 (2012) 171–178.
  - [15] Z. Jiang, G. Li, M. Zhang, A novel sensor based on bifunctional monomer molecularly imprinted film at graphene modified glassy carbon electrode for detecting traces of moxifloxacin, *RSC Adv.* 6 (2016) 32915–32921.
  - [16] A. Aghaei, M.R. Milani Hosseini, M. Najafi, A novel capacitive biosensor for cholesterol assay that uses an electropolymerized molecularly imprinted polymer, *Electrochim. Acta* 55 (2010) 1503–1508.
  - [17] H. Shekarchizadeh, A.A. Ensafi, M. Kadivar, Selective determination of sucrose based on electropolymerized molecularly imprinted polymer modified multiwall carbon nanotubes/glassy carbon electrode, *Mater. Sci. Eng. C* 33 (2013) 3553–3561.
  - [18] L. Chen, X. Wang, W. Lu, X. Wu, J. Li, Molecular imprinting: perspectives and applications, *Chem. Soc. Rev.* 45 (2016) 2137–2211.
  - [19] P.S. Sharma, A. Pietrzyk-Le, F. D'Souza, W. Kutner, Electrochemically synthesized polymers in molecular imprinting for chemical sensing, *Anal. Bioanal. Chem.* 402 (2012) 3177–3204.
  - [20] P. Liu, X. Zhang, W. Xu, C. Guo, S. Wang, Electrochemical sensor for the determination of brucine in human serum based on molecularly imprinted poly-o-phenylenediamine/SWNTs composite film, *Sens. Actuators B* 163 (2012) 84–89.
  - [21] X. Tan, Q. Hu, J. Wu, X. Li, P. Li, H. Yu, X. Li, F. Lei, Electrochemical sensor based on molecularly imprinted polymer reduced graphene oxide and gold nanoparticles modified electrode for detection of carbofuran, *Sens. Actuators B* 220 (2015) 216–221.
  - [22] M.J. Whitcombe, I. Chianella, L. Larcombe, S.A. Piletsky, J. Noble, R. Porter, A. Horgan, The rational development of molecularly imprinted polymer-based sensors for protein detection, *Chem. Soc. Rev.* 40 (2011) 1547–1571.
  - [23] B. Rezaei, M. Khalili Boroujeni, A.A. Ensafi, Caffeine electrochemical sensor using imprinted film as recognition element based on polypyrrole, sol-gel, and gold nanoparticles hybrid nanocomposite modified pencil graphite electrode, *Biosens. Bioelectron.* 60 (2014) 77–83.
  - [24] F. Wang, L. Zhu, J. Zhang, Electrochemical sensor for levofloxacin based on molecularly imprinted polypyrrole-graphene-gold nanoparticles modified electrode, *Sens. Actuators B* 192 (2014) 642–647.
  - [25] J.M. Pingarrón, P. Yáñez-Sedeño, A. González-Cortés, Gold nanoparticle-based electrochemical biosensors, *Electrochim. Acta* 53 (2008) 5848–5866.
  - [26] M.S. El-Deab, T. Ohsaka, An extraordinary electrocatalytic reduction of oxygen on gold nanoparticles-electrodeposited gold electrodes, *Electrochem. Commun.* 4 (2002) 288–292.
  - [27] E. Silveira, Vinhaça na geração de energia, *Rev. Fapesp* (2015) 68–71.
  - [28] O. Cavaletti, T.L. Junqueira, M.O.S. Dias, C.D.F. Jesus, P.E. Mantelatto, M.P. Cunha, H.C.J. Franco, T.F. Cardoso, R.M. Filho, C.E.V. Rossell, A. Bonomi, Environmental and economic assessment of sugarcane first generation biorefineries in Brazil, *Clean Technol. Environ. Policy* 14 (2012) 399–410.
  - [29] S.V. Prabhu, R.P. Baldwin, Electrocatalysis and detection of amino sugars, alditols, and acidic sugars at a copper-containing chemically modified electrode, *Anal. Chem.* 61 (1989) 2258–2263.
  - [30] B.J. Sanghavi, O.S. Wolfbeis, T. Hirsch, N.S. Swami, Nanomaterial-based electrochemical sensing of neurological drugs and neurotransmitters, *Mikrochim. Acta* 182 (2015) 1–41.
  - [31] K. Kamalodin Kor, Development and characterization of an electrochemical sensor for furosemide detection based on electropolymerized molecularly imprinted polymer, *Talanta* 146 (2016) 181–187.
  - [32] F.C.U. Santos, L.L. Paim, J. Luiz Da Silva, N.R. Stradiotto, Electrochemical determination of total reducing sugars from bioethanol production using glassy carbon electrode modified with graphene oxide containing copper nanoparticles, *Fuel* 163 (2016) 112–121.
  - [33] V.K. Gupta, N. Atar, M.L. Yola, Z. Üstündağ, L. Uzun, A novel magnetic Fe@Au core-shell nanoparticles anchored graphene oxide recyclable nanocatalyst for the reduction of nitrophenol compounds, *Water Res.* 48 (2014) 210–217.
  - [34] J. Wang, *Analytical Electrochemistry*, third ed., John Wiley & Sons, New Jersey, 2006.
  - [35] X. Dong, Y. Ma, G. Zhu, Y. Huang, J. Wang, M.B. Chan-Park, L. Wang, W. Huang, P. Chen, Synthesis of graphene-carbon nanotube hybrid foam and its use as a novel three-dimensional electrode for electrochemical sensing, *J. Mater. Chem.* 22 (2012) 17044–17048.
  - [36] [www.brasil.gov.br/economia-e-emprego/2016/04/safra-de-cana-2016-17-cresce-em-producao-e-area](http://www.brasil.gov.br/economia-e-emprego/2016/04/safra-de-cana-2016-17-cresce-em-producao-e-area) (accessed October 2016).
  - [37] Y. Fu, L. Zhang, G. Chen, Preparation of a carbon nanotube-copper nanoparticle hybrid by chemical reduction for use in the electrochemical sensing of carbohydrates, *Carbon* 50 (2012) 2563–2570.
  - [38] T.R.I. Cataldi, D. Centonze, I.G. Casella, E. Desimoni, Anion-exchange chromatography with electrochemical detection of alditols and sugars at a Cu<sub>2</sub>O-carbon composite electrode, *J. Chromatogr. A* 773 (1997) 115–121.
  - [39] I.G. Casella, T.R.I. Cataldi, A.M. Salvi, E. Desimoni, Electrocatalytic oxidation and liquid chromatographic detection of aliphatic alcohols at a nickel-based glassy carbon modified electrode, *Anal. Chem.* 65 (1993) 3143–3150.
  - [40] K. Tang, L. Liang, Y. Cai, S. Mou, Determination of sugars and alditols in tobacco with high performance anion-exchange chromatography, *J. Sep. Sci.* 30 (2007) 2160–2166.